SBS Gain Suppression in a Passive Single-Mode Optical Fiber by the Multi-Mode Acoustic Waveguide Design

Sergey V. Tsvetkov, Maxim M. Khudyakov, Alexey S. Lobanov, Denis S. Lipatov, Mikhail M. Bubnov, Alexey N. Guryanov, Valery Temyanko, and Mikhail E. Likhachev

***Abstract*—A novel method of stimulated Brillouin scattering (SBS) gain suppression in passive single-mode optical fibers is proposed and experimentally verified. The effect is achieved due to special propagation conditions created for a number of the core-bounded acoustic modes effectively involved in the SBS, such that its gain becomes approximately evenly distributed over a wide spectral range, thereby proportionally reducing its maximum. To verify and investigate this method in depth, single-mode large-mode-area (LMA) fibers with correspondingly optimized acoustic index profiles are fabricated, experimentally tested, and analyzed. Uneven complex doping of the core with two additives, P_2O_5 and F, forms a high-contrast gradient acoustic index profile while maintaining a quasi-uniform optical refractive index profile. With a contrast of P_2O_5 of more than 6 mol.%, we achieved 8 dB of SBS suppression over conventional uniformly doped LMA fibers. Moreover, it is shown that more than 10 dB of SBS gain suppression can be achieved if the optimal dopant distribution is realized.**

***Index Terms*—Acoustic index profile, Brillouin gain spectrum, fiber acoustic modes, SBS gain suppression, single-mode optical fibers, stimulated Brillouin scattering.**

I. Introduction

STIMULATED Brillouin scattering (SBS) is the major factor limiting the maximal power of narrow-band (less than 100 MHz in linewidth) fiber lasers. There are many efficient methods to reduce SBS gain in optical fibers by using variations in temperature, stress, dopant concentration, or the core radius along the fiber length [1]–[3]. However, these methods are quite complicated and have limited applicability.

Recently, considerable attention has been paid to the development of new methods allowing SBS suppression in longitudinally uniform optical fibers. Most of these methods are based on the well-known fact that the doping of silica glass controls not only the refractive index profile (RIP) for the optic wave but also the acoustic index profile (AIP) for the acoustic wave [4]. Using the codoping technique with two or more dopants [5] acting differently on optic and acoustic refractive indices, one can induce a transversely varying AIP, which can result in a sufficient reduction in the interaction between acoustic and optic waves, and, correspondingly, the SBS gain [6]. As shown in [7], [8], a specially curved ramp-like AIP can reduce the SBS gain (or, accordingly, raise the SBS power threshold) by an order of magnitude or more. Such a design was first realized experimentally using Al_2O_3–GeO_2–Yb codoping of the silica core surrounded by a wide acoustically dense GeO_2-doped ring (pedestal) [9]. Since Al_2O_3, residing mostly in the core center, reduces the acoustic index of the silica, the energy of the optical wave was localized in the single-mode core region, whereas the energy of acoustic modes is localized mainly in the multi-mode region of the pedestal, which made it possible to achieve strong SBS gain reduction in comparison with the ordinary (step-indexed AIP) passive GeO_2-doped large-mode-area (LMA) fiber. However, for passive single-mode fibers, the presence of the large pedestal structure is undesirable, especially when including additional fiber cladding structures, e.g., stress-applying parts [10]. In addition, without it, the Al_2O_3–GeO_2-doped "anti-guide" acoustic structures provide a rather small SBS suppression effect (despite optimization, no more than 4.3 dB [11]) due to the increasing domination of the leaky acoustic modes in the Brillouin gain spectrum (BGS) [12].

To overcome such problems, we propose a novel design of SBS-suppressed fibers, in which the core RIPs and AIPs are controlled by two dopants with opposite signs of optic refractivity, but both dopants increase the acoustic index. Recently, complex doping with P_2O_5–F has received attention [5], [25]. Due to relatively high molar concentrations of P_2O_5 ($\sim$13 mol.%) and F ($\sim$7 mol.%), practically achieved with the modified chemical

Manuscript received August 30, 2020; accepted October 13, 2020. Date of publication October 16, 2020; date of current version January 15, 2021. This work was supported by the Russian Science Foundation under Project 18-19-00687. *(Corresponding author: Sergey V. Tsvetkov.)*

Sergey V. Tsvetkov, Mikhail M. Bubnov, and Mikhail E. Likhachev are with the Prokhorov General Physics Institute of the Russian Academy of Sciences, Dianov Fiber Optics Research Center, Moscow 119333, Russia (e-mail: science@fopts.ru; bubnov@fo.gpi.ru; likhachev@fo.gpi.ru).

Maxim M. Khudyakov is with the Prokhorov General Physics Institute of the Russian Academy of Sciences, Dianov Fiber Optics Research Center, Moscow 119333, Russia, and also with the Moscow Institute of Physics and Technology (State University), Dolgoprudny 141700, Russia (e-mail: mkhudyakov@fo.gpi.ru).

Alexey S. Lobanov and Alexey N. Guryanov are with the Institute of Chemistry of High Purity Substances of the Russian Academy of Sciences, Nizhny Novgorod 603950, Russia (e-mail: lobanov@ihps-nnov.ru; guryanov@ihps-nnov.ru).

Denis S. Lipatov is with the Institute of Chemistry of High Purity Substances of the Russian Academy of Sciences, Nizhny Novgorod 603950, Russia, and also with the Prokhorov General Physics Institute of the Russian Academy of Sciences, Dianov Fiber Optics Research Center, Moscow 119333, Russia (e-mail: lipatov@ihps-nnov.ru).

Valery Temyanko is with the College of Optical Sciences, University of Arizona, Tucson, AZ 85721 USA (e-mail: vtemyanko@optics.arizona.edu).

Color versions of one or more of the figures in this article are available online at https://ieeexplore.ieee.org.

Digital Object Identifier 10.1109/JLT.2020.3031726

vapor deposition (MCVD) technology, a rather high acoustic index contrast can be obtained with this approach, which increases the number of acoustic modes and widely distributes their eigenfrequencies over the BGS.

In this paper, we theoretically and experimentally investigate the BGS properties of acoustically multi-mode and optically single-mode LMA fibers, aiming predominantly to the optimal AIP parameters giving the widest and homogeneous BGS, which corresponds to the maximal SBS gain suppression. In contrast to a standard passive fiber with similar optical parameters, a strictly single-mode pedestal-free LMA fiber providing more than 8 dB of SBS gain reduction was fabricated for the first time. It is shown that an even larger SBS gain suppression could be achieved by using a special gradient-increasing AIP and by increasing the dopant concentration contract.

II. Theoretical Concept

During the SBS process, backscattered Stokes radiation is generated due to a coherent interaction between the pump light and electrostrictively induced acoustic waves [14]. In a weakly guiding optical fiber, neglecting losses and depletion of the narrow-line pump power $P_{\rm p}$, the z-axis evolution of the spectral power density $P_{\rm S}$ of the Stokes wave, propagating in the backward direction, is driven by equation [15]

$$\frac{\partial}{\partial z}P_{\rm S}+\frac{g_{\rm B}(\Omega)}{A_{\rm eff}}P_{\rm p}P_{\rm S}=0 \tag{1}$$

where $g_{\rm B}(\Omega)$ is the frequency-dependent SBS gain coefficient, $A_{\rm eff}$ is the optic effective mode area, and Ω is the acoustic frequency (called the Brillouin frequency), defined as the difference between the pump $\nu_{\rm P}$ and Stokes $\nu_{\rm S}$ frequencies [14]

$$\Omega=\nu_{\rm p}-\nu_{\rm S}\approx 2n_{\rm eff}V_{\rm A}\nu_{\rm p}/c=2n_{\rm eff}V_{\rm A}/\lambda \tag{2}$$

where $V_{\rm A}$ is the speed of the acoustic wave, $n_{\rm eff}$ is the effective refractive index of the optic mode, λ is the pump wavelength, and c is the speed of light in vacuum. In the absence of cross-modulation, the BGS is formed by independent contributions from acoustic modes with different frequencies, into which the thermally originated Brillouin acoustic wave field can be expanded [6]. If only one acoustic mode prevails in this expansion, a narrow quasi-single-line Stokes power spectrum centered at $\nu_{\rm S}$ is obtained. The transverse distribution of the Stokes intensity depends only on the RIP, and the acoustic modes are orthogonal to each other. Therefore, the Stokes scattered power can be evenly redistributed between the set of M spectral lines, allowing a damped proportional Brillouin gain (Fig. 1).

Consider an ordinary single-mode LMA fiber with a core radius $a=7$ μm, as shown in Fig. 2(a). The core has essentially homogeneous RIP and AIP. We define the latter, for consistency with the optical refractive index contrast profile $\Delta n(r)$, as the acoustic refractive index contrast profile

$$\Delta N(r)=V_{\rm c}/V_{\rm A}(r)-1 \tag{3}$$

where $V_{\rm A}(r)$ is the transverse acoustic velocity profile and $V_{\rm c}$ is the speed of the longitudinal sound wave in the outer cladding medium (for the pure fused silica, at $\lambda=1.55$ μm, $V_{\rm c}=5944$ m/s [6]).

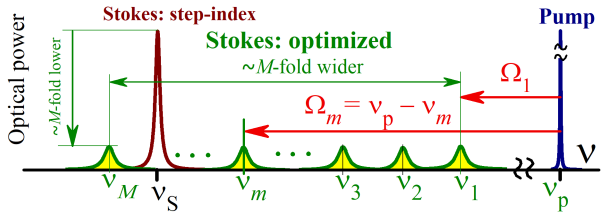

Fig. 1. Scheme of the concept of multi-mode SBS suppression; ν is the optic frequency, and Ω is the Brillouin frequency increasing in the opposite direction.

In the CW regime, both the pump and Stokes radiation propagate only as one core-bounded transverse fiber mode $\rm LP_{01}$ (neglecting a polarization), characterized by the nearly Gaussian radial intensity distribution $|E|^2$ with $A_{\rm eff}\approx 200\mu{\rm m}^2$ at $\lambda=1.55$ μm. In contrast, the Brillouin acoustic wave consists of 5 core-guided modes ξ_1–ξ_5. Generally, each acoustic mode has its own resonant Brillouin frequency Ω_m (see Fig. 1), whereas the corresponding field distribution $\xi_m(r)$ is a solution to the scalar eigenvalue equation (the azimuthal symmetry of the optic and acoustic fields is assumed) [17]

$$\left(\frac{d^2}{dr^2}+\frac{1}{r}\frac{d}{dr}\right)\xi_m+4\pi^2\left[\frac{\Omega_m^2}{V_{\rm A}^2(r)}-4\frac{\nu_{\rm p}^2}{c^2}n_{\rm eff}^2\right]\xi_m=0 \tag{4}$$

If the spontaneous excitation coefficient of the mth acoustic mode is proportional to the overlap radial integral I_m^{ao} between the normalized acoustic mode field $\xi_m(r)$ and the pump intensity distribution [18], then a BGS can be described by the multi-Lorentzian form [6]:

$$g_{\rm B}(\Omega)=\frac{4\pi n_{\rm eff}^8 p_{12}^2}{c\rho\lambda^3\Delta\Omega}\sum_m\frac{(I_m^{ao})^2}{\Omega_m}\frac{(\Delta\Omega/2)^2}{(\Omega-\Omega_m)^2+(\Delta\Omega/2)^2} \tag{5}$$

$$I_m^{ao}=\int_0^\infty|E|^2\xi_m r dr\Big/\left(\int_0^\infty|E|^4 r dr\int_0^\infty\xi_m^2 r dr\right) \tag{6}$$

where p_{12} is the elasto-optic coefficient (taken as 0.252 for silica [19]) and ρ is the mean value of the material density (taken as 2200 kg/m^3 for the doped fused silica). $\Delta\Omega$ is the single BGS line width (by FWHM) (the inverse of acoustic wave damping time) assumed to be the same for all acoustic modes, which affects the spectral peak sharpness and height; in this section, it is taken as 45 MHz (the average between that for GeO_2- and P_2O_5-doped silica [22], [23]).

Fig. 2(a) shows that the first mode ξ_1 has a distribution very similar to the optic intensity profile and, thus, has the largest overlap integral $I_1^{ao}\approx 0.979$, whereas the absolute values of the overlap integrals of other modes are less than 0.1. According to (5), the summary impact of other modes are almost negligible, producing a single-line BGS $g_{\rm B}(\Omega)$ with a maximum at ≈14 pm/W at Ω_1 ≈10.9GHz (Fig. 2(b)).

A different result is observed when the AIP is altered in the "M"-shaped manner but the RIP is preserved. As an example, as shown in Figs. 2(c) and 2(d), a 5-fold linear change in the acoustic index contrast allows the propagation of a total of 9 guided acoustic modes, of which the first 7 modes have considerable overlap integrals much more comparable with each

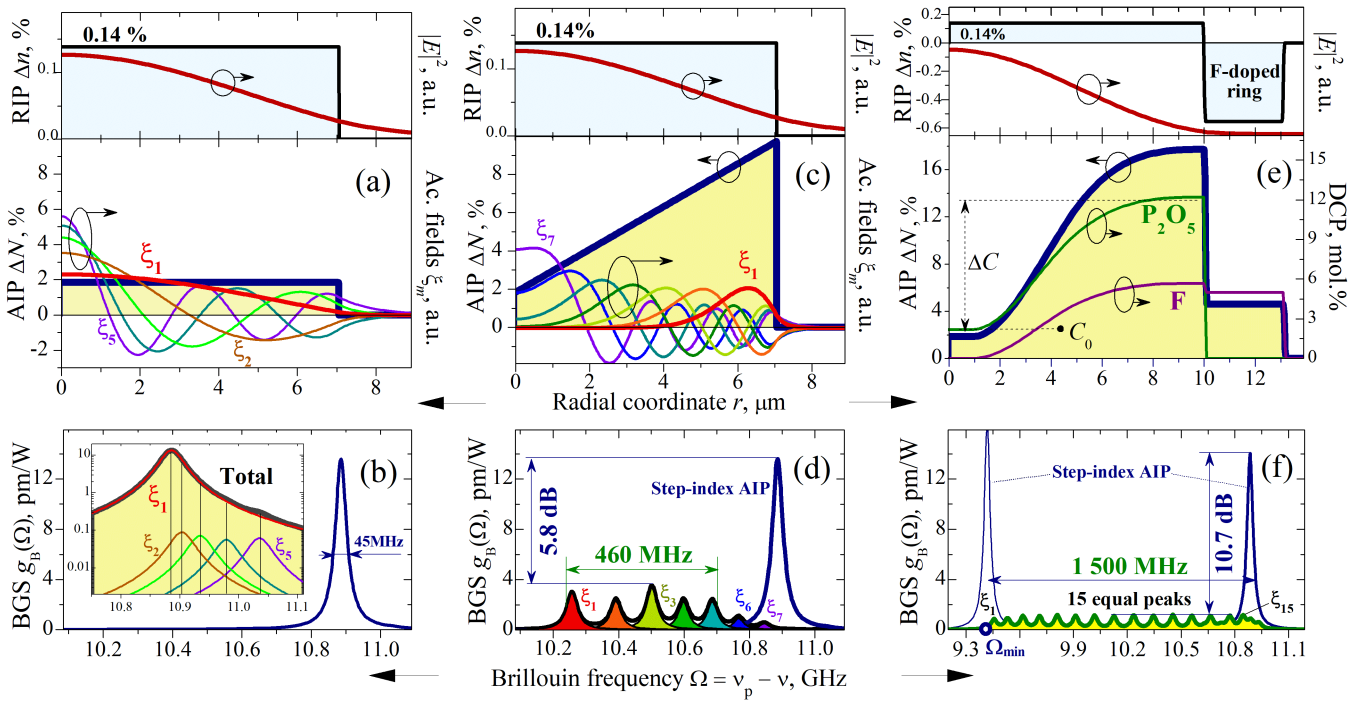

Fig. 2. (a) Step-index RIP and AIP with 7 μm core radius, the optic intensity $|E|^2$ and normalized acoustic fields ξ_m of the ordinary homogeneously doped LMA fiber; (b) the BGS corresponding to the fiber in (a), in the inset: the log-scaled BGS view along with individual BGSs for each acoustic mode, revealing a domination of the first mode ξ_1; (c) the "M"-shaped AIP with normalized fields of 7 corresponding acoustic modes, for which the RIP and optic intensity are the same; (d) the 7-peak BGS enveloping the individual impacts of acoustic modes (filled) corresponding to the fiber in (c), in comparison with that of the fiber in (a); (e) the ideal optimized nonlinearly increasing AIP and the corresponding concentration profiles of the basic P_2O_5 and secondary F dopants of the single-mode LMA fiber with the step-index RIP with an enlarged 10μm core radius due to the F-doped 3μm-thick ring cladding; (f) the corresponding optimized 15-peak BGS from 21 modes in comparison with the BGSs for the same fiber with the step-index core AIP with $\Delta N \approx 1.8\%$ (right peak) and $\Delta N \approx 18\%$ (left peak).

other than with the other modes (the RMS value is ~0.4). From Fig. 2c, one can observe that the maximum of the distribution of the ξ_1 mode is considerably shifted toward the core border, and thus, the overlap integral I_1^{ao} decreases twice since the optical intensity fades quite rapidly in this region, producing the corresponding four-fold reduction in the SBS gain at this mode. For the higher-order modes ξ_2–ξ_5, the overlap integrals, in contrast, are approximately 5 times greater because the areas under the negative parts of their fields are substantially reduced compared to those of the step-index case. Fig. 2d shows that the BGS is broadened in the positive frequency range by more than an order of magnitude (by FWHM) and obtains 7 distinct lines spanned by approximately 100 MHz. The maximum gain value of 3.55 pm/W at $\Omega_3 \approx$10.5 GHz, related to the ξ_3 mode having the largest overlap integral $I_3^{ao} \approx 0.477$, provides a 5.8 dB reduction in the SBS gain compared to the step-index AIP.

As mentioned above, two different dopants can be used to obtain a change in the core AIP independently of the RIP. The first one (we call it the basic dopant) initially defines the desired positive optic refractive index contrast Δn with the waveguiding shape of the AIP. Therefore, this dopant (for example, P_2O_5 or GeO_2 can be used) will raise both the optic and acoustic refractivities of the silica. The second dopant (we call it the secondary dopant) is chosen to compensate for the increase in the optic refractive index from the basic along with a further increase in the acoustic refractive index contrast ΔN (for such a purpose, F or B_2O_3 can be used). The results obtained with the "M"-shaped AIP can be sufficiently improved if we use a nonlinear radial change in the dopant concentrations. When adjusting the dopant concentration profiles (DCPs) of the basic and secondary dopants, we assume the additive approximation (appropriate for relatively small Δn) [17]

$$\Delta n\,(r) = R_1 C_1\,(r) + R_2 C_2\,(r) \tag{7}$$

where R_j and C_j are the molar refractivity and concentration of the jth dopant, respectively. Accordingly, the AIP $\Delta N(r)$ can be obtained as follows

$$\Delta N\,(r) = \frac{K_1 C_1\,(r) + K_2 C_2\,(r)}{1 - K_1 C_1\,(r) - K_2 C_2\,(r)} \tag{8}$$

which is derived from (3) with the use of the similar additive model for the longitudinal acoustic velocity

$$V_{\mathrm{A}}\,(r) = V_c\,(1 - K_1 C_1\,(r) - K_2 C_2\,(r)) \tag{9}$$

where the coefficients K_j are the molar acoustic velocity coefficients of the corresponding dopants.

An additional depressed-optical-index ring made of the secondary dopant can also be added next to the core to shift the single-mode cutoff toward larger values of the core radius and additionally increase the number of acoustic modes.

Fig. 2(e) shows the abstract optimized (*idealized*) AIP along with the corresponding DCPs of the single-mode LMA fiber with

$A_{\rm eff} = 200\mu{\rm m}^2$. The 3 μm-thick 5 mol.% F-doped ring allowed enlargement of the core radius up to 10 μm. The values C_0 and ΔC are introduced to determine the central and maximal contrasts of the basic dopant concentration, respectively. According to (7) and (8), the corresponding maximum for the secondary dopant is also proportional to ΔC. The detailed analysis of the SBS gain suppression dependency on ΔC is presented in the Discussion. The shape of the AIP is similar to that obtained in [7], [8] using beam-propagation methods for the optimized flat-top BGS. Fig. 2(f) shows the corresponding optimized BGS. Due to the 16% change in ΔN and the optimally curved AIP shape, 15 spectral lines (related to the first 15 modes from a total of 21 modes) are spanned by ~100 MHz, resulting in 1500 MHz FWHM and a maximal SBS gain value of 1.2 pm/W. The SBS gain for the appropriate step-index AIP, formed by uniform core doping with C_0, is ≈14pm/W at ≈10.86 GHz (mode ξ_4 from a total of 11 modes, $I_4^{ao} \approx 0.991$), which gives 10.7 dB of SBS suppression for the optimized AIP. In addition, the same step-index AIP can be formed by homogeneous codoping with maximal values of the basic and secondary dopants. However, among the 27 supported guided modes, only the ξ_1 mode with $I_1^{ao} \approx 0.990$ sharply peaks to 16.3 pm/W at the lower frequency bound $\Omega_{\rm min} = 9.42$ GHz. This example demonstrates the crucial role of AIP shaping in multi-mode SBS suppression.

III. Experiment and Simulations

To verify the concept presented above, we fabricated several special LMA fibers with gradually increasing AIPs and relatively homogeneous RIPs of the core surrounded by a fluorine-doped ring to increase its radius a and, correspondingly, the number of acoustic modes. The fiber preforms were fabricated by MCVD technology using P_2O_5 and F as the basic and secondary dopants, respectively. This dopant choice was dictated by the possibility of the simultaneous introduction of higher concentrations of both dopants [13] than a pair of GeO_2 and F dopants can obtained. We do not use B_2O_3 as the secondary dopant since it creates strong stresses in the core, which limits the possible applications of such fibers.

The preforms were drawn into LMA fibers, over which, using electron microscopy, a quantitative analysis of the dopant contents was carried out, and actual DCPs were obtained. Using these data, along with the experimental measurements, simulations of the BGSs were performed. For this purpose, according to (6–8), we used the following known optic and acoustic coefficients for P_2O_5, GeO_2 and F, respectively: $R_{\rm P2O5} \approx 0.9\times10^{-3}({\rm mol.\%})^{-1}$ [20] and $K_{\rm P2O5} \approx 8.4\times10^{-3}({\rm mol.\%})^{-1}$, $R_{\rm GeO2} \approx 1.47\times10^{-3}({\rm mol.\%})^{-1}$ [21] and $K_{\rm GeO2} \approx 1.14\times10^{-3}({\rm mol.\%})^{-1}$ [6], and $R_{\rm F} \approx -1.6\times10^{-3}({\rm mol.\%})^{-1}$ [24] and $K_{\rm F} \approx 8.8\times10^{-3}({\rm mol.\%})^{-1}$[6], [22].

Here, we present the results obtained for two special LMA fibers designated *Fiber-I* and *Fiber-II*. Another typical LMA fiber doped primarily with GeO_2 (and some amount of fluorine to lower the core refractive index difference) is used for comparison of the experimental SBS characteristics and thus designated *Control*. The parameters of all three fibers are given in Table I. The SBS gain $g_{\rm B}$ for each fiber was obtained in two independent ways: from measurements of the BGS $g_{\rm B}(\Omega)$ and from the threshold power $P_{\rm th}$.

TABLE I
Parameters of the Tested Fibers

Fiber	<Δ*n*> of the core	*a*, μm	$A_{\rm eff}$, μm^2	$\lambda_{\rm cutoff}$, μm	Δ*C*, mol.%
Fiber-I	2.8×10^{-3}	7.8	135	1.33	2.8
Fiber-II	1.9×10^{-3}	13.5	345	1.54	3.0
Control	1.4×10^{-3}	10	323	1.54	0.0

For the BGS measurements, the pump-probe method was used with a setup similar to that described in [11], taking into account that at a moderate $P_{\rm p}\sim 1$ W pump level and a relatively short fiber length $L \sim 100$ m, the cross-modulation effects are negligible. A weak narrow-line ~1 MHz probe signal of the intensity $I_{\rm L}$ from the laser diode source is sent after the electro-optic modulator toward the pump from the opposite end of the test fiber, and it acquires, through the phase-matched component of the Brillouin pump-induced acoustic wave, a certain gain corresponding to the intensity I_0 measured at the pump-input fiber end. Thus, the gain spectrum is obtained as a result of tracing the range of the probe frequency modulation. With the loss coefficient α, the Brillouin gain coefficient $g_{\rm B}{}^{\rm BGS}$ is then determined from the well-known formula [15] $I_0 = I_{\rm L}\cdot\exp(g_{\rm B}{}^{\rm BGS} P_{\rm p}L_{\rm eff}/A_{\rm eff} - \alpha L)$, where $L_{\rm eff} = [1 - \exp(-\alpha L)]/\alpha$ is the effective fiber length depending on the small-power loss coefficient α. The corresponding results are shown on the left-hand side of Table II.

The SBS pump threshold powers were estimated by observing the known effect of the SBS-induced pulse instability [15]. Each test fiber was 4 m long ($L_{\rm eff} \approx L$) and was pumped with circularly polarized pulses of 100 ns width at the repetition rate of 13.33 kHz for Fiber-I and Fiber-II and 50 kHz for the control Ge–F fiber. Such conditions provided a quasiCW operational regime. The peak $P_{\rm th}$ pump threshold power was detected at the first noticeable instability of the trailing edge of the pump pulse [25] using a setup similar to that described in [26]. We then estimated the SBS gain as $g_{\rm B}{}^{\rm th} \approx 21\times A_{\rm eff}/(P_{\rm th}L_{\rm eff})\times 1.5$ [27], where a factor of 1.5 takes into account the uncontrolled evolution of the polarization state of the light in the low-birefringent fiber being tested [28]. Finally, we calculated the corresponding SBS suppression ratios $SR_{\rm th}$ relative to the SBS gain of the Control fiber. The corresponding results are summarized on the right-hand side of Table II. Clearly, the values $g_{\rm B}{}^{\rm BGS}$ and $g_{\rm B}{}^{\rm th}$ obtained from the BGS and power threshold approaches, respectively, are sufficiently similar.

The main goal of the experiment with Fiber-I was to verify that a gradually increasing shape of the AIP within the core area can create a multi-mode BGS structure exhibiting at least several spectral peaks with comparable heights and induce the corresponding widening of its FWHM. To obtain a good resolution of the BGS fine modal structure, the core radius $a = 7.8$ μm was intentionally chosen to be not too large, taking into account the ~5 mol.% F-doped ring. The electron microscope analysis revealed that the P_2O_5 dopant concentration reaches a maximum of 6.3 mol.% near the core boundary, with the corresponding F

TABLE II
SBS SPECTRUM AND THRESHOLD CHARACTERISTICS

Fiber	BGS characteristics[a]					Power threshold characteristics		
	g_B^{BGS}, pm/W	SR_{BGS}, dB[b]	$\Delta\Omega$, MHz	FWHM, MHz	M_{total}	P_{th}, W	g_B^{th}, pm/W	SR_{th}, dB[b]
Fiber-I	2.5	8.0	58	258	*13*	465	2.3	8.1
Fiber-II	2.5	8.0	58	290	*23*	1275	2.3	8.1
Fiber-II-optim	*1.3*	*10.8*	*57*[c]	*580*	*23*	–	–	–
Control fiber	15.8	0.0	35	35	*12*	194	14.7	0.0

[a]Values obtained via simulations are shown in *Italics*. [b]SR_{BGS} and SR_{th} are related to the Control fiber. [c]From [22].

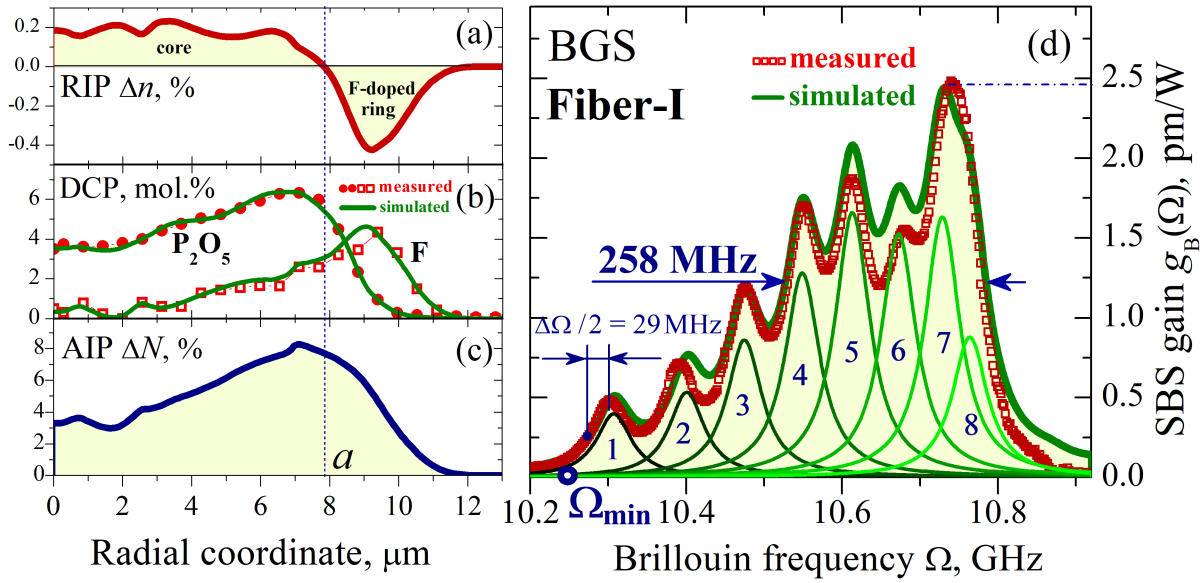

Fig. 3. (a) The actual RIP of Fiber-I having the core NA ≈ 0.09; (b) the corresponding DCPs measured (dots) and simulated (solid lines); (c) the corresponding actual AIP with a quasitriangular shape, close to that in Fig. 2(c), except the noticeable trough at approximately 2 μm "pushed " the 7th mode peak up; (d) the measured multipeak BGS for Fiber-I (square dots); additionally, the simulated BGS is plotted (solid) with the individual spectral impacts of the acoustic modes numbered, verifying the acoustic modal structure in the measured spectrum.

dopant concentration of 2.6 mol.%. Using the above acoustic coefficients with the value of $n_{eff} \approx 1.44539$ at $\lambda = 1.55$ μm, we simulated the BGS, trying to build the fiber model to replicate measured DCP data as closely as possible. The results shown in Fig. 3 reveal that Fiber-I (NA ≈ 0.09) supports 8 (from $M_{total} = 13$) guided acoustic modes of the zeroth azimuth order, having significant overlap integrals with the optic field intensity. Among them, 5 modes, from the 4th to the 8th, form the principal part of the BGS with the FWHM equal to 258 MHz, which is 4.5 times wider than that of the single Brillouin line. The envelope of the measured BGS (dotted) is in good agreement with the simulated BGS. Moreover, the leftmost maximum of the measured BGS allowed us to verify the width $\Delta\Omega$ of the single Brillouin line in P_2O_5–F-doped silica fibers, since it strictly corresponds to one acoustic mode. As shown in Fig. 3(b), $\Delta\Omega \approx 58$ MHz, which matches the corresponding value of approximately 57 MHz published in [22] and is 1.6 times larger than that of the GeO_2-doped fiber [23]. The rightmost BGS peak formed by the 7th and 8th modes (which is therefore noticeably wider than other peaks) is the highest peak and thus determines the value of $g_B^{BGS} = 2.5$ pm/W, which, in turn, defines the SBS threshold or SBS suppression ratio SR_{BGS}. Of course, the latter also depends on the Brillouin gain of a reference fiber. In our case, the Control fiber supporting a comparable number of acoustic modes $M_{total} = 12$ (see the RIP and BGS in Fig. 4(a) and 4(e), respectively) provided a measured gain of $g_B^{BGS} = 15.8$ pm/W, which gives $SR_{BGS} \approx 8$dB. Comparing the gains g_B^{th} obtained from the threshold powers, we obtain the similar result of $SR_{th} \approx 8.1$ dB.

In the second experiment with Fiber-II, we tried to achieve, within our technological MCVD capabilities, the best single-mode LMA structure of Fiber-I, reaching the maximum possible number of guided acoustic modes. Comparing Figs. 3(b) and 4(c), we were able to raise the concentration of fluorine within the core region by approximately 1.5-fold, trying to maintain the shapes of the DCPs close to those in Fig. 2(e). Thus, the average optic refractive index contrast $<\Delta n>$ became closer to that of the control fiber, and the core radius was increased by nearly 75%. As a result, Fiber-II supports $M_{total} = 23$ acoustic modes, almost twice as many as Fiber-I or the Control fiber. However, due to unavoidable technological imperfections, the SBS gain g_B^{BGS} of Fiber-II appeared to be the same as that of Fiber-I, although the BGS shown in Fig. 4(e) is changed sufficiently. Due to the 2-fold increase in the spectral mode density, individual mode peaks became almost unresolvable, whereas due to few

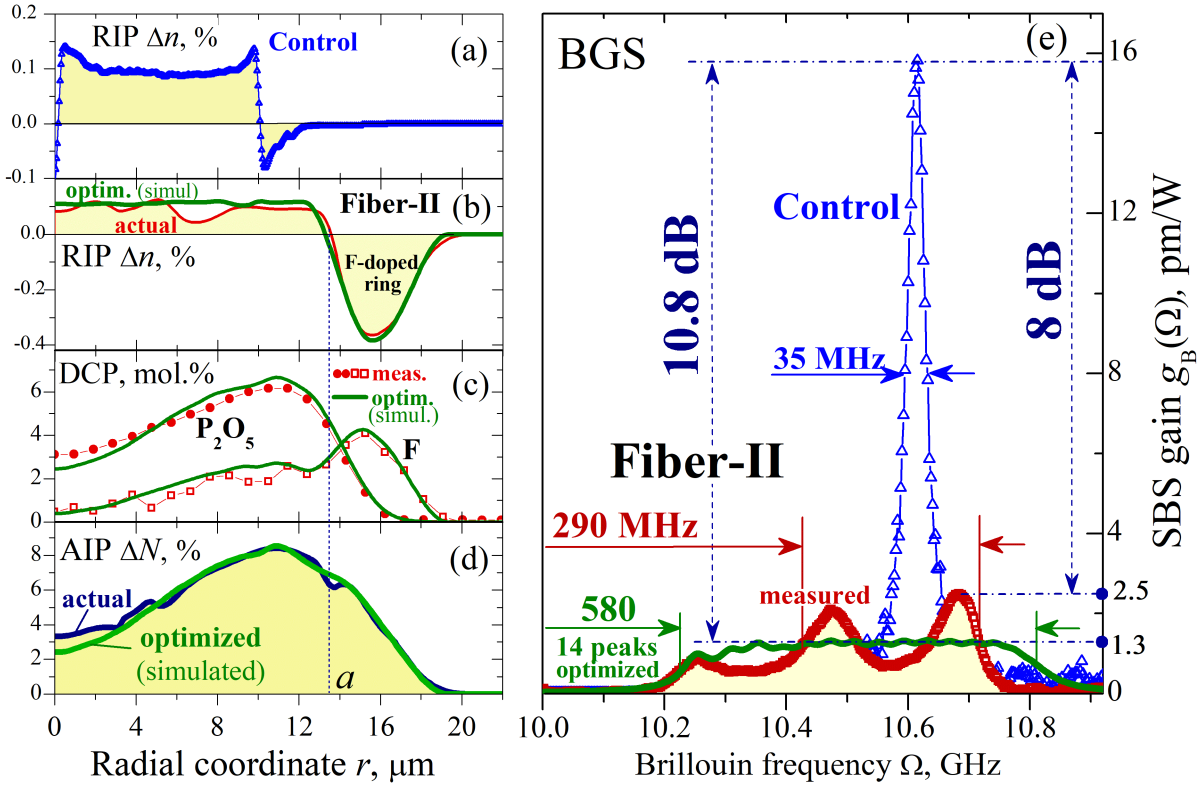

Fig. 4. (a) The measured RIP for the Control Ge–F fiber with NA ≈ 0.064; (b) the actual RIP of Fiber-II, and the optimized RIP of Fiber-II-optim, both with the core NA ≈ 0.074; (c) corresponding DCPs measured (dots) for Fiber-II, and the optimized (solid lines) for Fiber-II-optim; (d) the slightly imperfect actual and optimized corresponding AIPs; (e) the measured 3-peak BGS for Fiber-II along with the optimized (simulated) 14-peak BGS for the Fiber-II-optim model and the measured BGS (triangular dots) for the Control fiber.

relatively small defects of the actual AIP in the central half of the fiber core (Fig. 4(d)), the BGS acquired two relatively high peaks at approximately 10.47GHz and 10.68GHz. The latter peak gave $g_B{}^{BGS} = 2.5$ pm/W, which is also confirmed by measuring the threshold power with $g_B{}^{th} = 2.3$ pm/W. A general skew of the BGS to the right is due to deviation of the average slope of the P_2O_5 DCP from the optimum.

Since, at this time, the practical tailoring of ideal DCPs is challenging, we simulated the possibly achievable BGS if the mentioned drawbacks from the DCPs were eliminated. The results, designated *Fiber-II-optim*, are also shown in Table II, and the optimal BGS with 14 similar peaks is plotted in the inset of Fig. 4(e). Therefore, compared to the results of the Control fiber, with *Fiber-II-optim*, the BGS FWHM doubles to 580 MHz, and the SBS gain can be correspondingly reduced to 1.3 pm/W, resulting in a SR_{BGS} of up to 10.8 dB.

IV. Discussion

Considering the experimental and simulated results, which were similar, we see that if the core AIP is optimized and its RIP is close to uniform, the main factor affecting the amount of SBS suppression in the optimized LMA fibers is the maximal contrast ΔC of the basic dopant concentration. To show the dependency of the SBS suppression ratio SR on ΔC for P_2O_5, we have chosen the *idealized* step-index model of the LMA fiber (Fig. 2(e)),

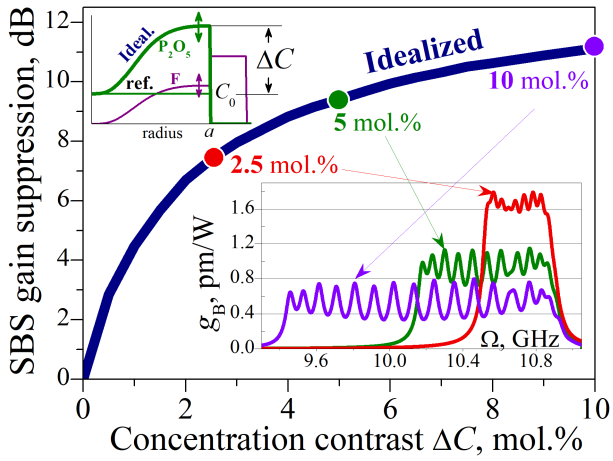

Fig. 5. Dependency of the SBS gain suppression ratio on a maximum concentration contrast ΔC of P_2O_5 for the idealized model relative to the similar optical fiber with a uniformly P_2O_5-doped core with the value C_0; at each point, only the core concentrations of F are changed proportionally according to ΔC, which keeps the RIPs and relative shape parameters of the DCPs unchanged. In the inset: the corresponding evolution of the BGS.

wherein ΔC is changing from 0 to 10 mol.%, providing up to 11 dB of SBS suppression (Fig. 5). The fluorine concentrations are scaled proportionally within the core radius a to keep the core RIP unchanged. The SBS suppression ratio is determined

as $SR(\Delta C) = {g_{\rm B}}^{\rm max}(\Delta C)/{g_{\rm B}}^{\rm Ref}$, where ${g_{\rm B}}^{\rm Ref}$ is the SBS gain of a reference fiber, having the uniform core AIP, and all other parameters are exactly the same as in the optimized fiber. Note that in the experimental investigations, we used the specific estimates of the *SR* determined by comparing the measured values of ${g_{\rm B}}^{\rm BGS}$ obtained for the P_2O_5–F-doped test fibers with that for the Ge–F-doped *Control* fiber. Therefore, if we use the latter as a reference here, the values of $SR(\Delta C)$ become larger in $\Delta\Omega_{\rm P2O5}/\Delta\Omega_{\rm GeO2} = 57$ MHz/35 MHz ≈ 1.6 times (2 dB).

As one can note from the inset of Fig. 5, the BGS FWHM proportionally increases with ΔC at a rate of $\sim$150 mol.%$^{-1}$. However, the number of BGS peaks (7, 11 and 16 for $\Delta C = 2.5$, 5 and 10 mol.%, respectively), corresponding to the acoustic modes effectively involved in the SBS, increases nonlinearly with ΔC, providing a somewhat lower SBS suppression ratio than the inverse of the total number of acoustic modes $M_{\rm total}$. This is a unique feature of LMA fibers with relatively dense acoustic multimodal spectra, whereas high-NA small-core fibers have only several acoustic modes with relatively large frequency distances between them. As seen from the BGS results in Fig. 3(b), the SBS gain at each eigenfrequency Ω_m is additionally increased by contributions of the neighboring lobes, producing a certain damping action on the BGS maximum.

A change in the core radius a within the single-mode regime affects the SBS gain suppression ratio and ΔC in a similar way. In contrast, the FWHM changes insufficiently due to saturation of the lowest mode eigenfrequency at relatively large core radius values.

In summary, we note that any deviation of the doping profile from the ideal (even for one of the additives) is reflected accordingly in the BGS: even a relatively small flattened region of the smoothly increasing optimized AIP can sharply boost the spectral impact of a certain acoustic mode and dampens the impacts of others. The greatest problems, in this regard, come from the higher-order acoustic modes, which form the right-hand side of the BGS (see, e.g., Figs. 3(b) and 3(d)). Their fields have a large number of oscillations and therefore, together with the corresponding acousto-optic integrals, are very sensitive to changes in the AIP, especially in its central part.

V. Conclusion

Considering the theoretical and experimental results, we see that the multi-mode acoustic guiding regime carries a large potential for SBS gain suppression. The simulations, based on the measured parameters obtained from the experiments, showed that with a certain technological improvement, at least in the precision control of complex doping, about an order of SBS gain reduction can be achieved with respect to the performance of ordinary LMA fibers. Moreover, if one could increase the maximal core dopant contrast ΔC up to 10 mol.%, this factor can be increased to 11–13 dB depending on the reference. In addition, it has been found and quantitatively confirmed that different LMA fibers of similar compounds exhibit nearly the same SBS suppression ratio versus ΔC or the BGS FWHM, which can be useful for practical characterization of the SBS suppression properties of fibers made using this novel approach.

References

[1] M. Ohashi and M. Tateda, "Design of strain-free fiber with nonuniform dopant concentration for stimulated brillouin scattering suppression," *J. Lightw. Technol.*, vol. 11, no. 12, pp. 1941–1945, Dec. 1993.

[2] A. Liu, "Suppressing stimulated brillouin scattering in fiber amplifiers using nonuniform fiber and temperature gradient," *Opt. Express*, vol. 15, pp. 977–984, 2007.

[3] K. Shiraki, M. Ohashi, and M. Tateda, "Suppression of stimulated brillouin scattering in a fibre by changing the core radius," *Electron. Lett.*, vol. 31, pp. 668–669, 1995.

[4] P. J. Thomas, N. L. Rowell, H. M. van Driel, and G. I. Stegeman, "Normal acoustic modes and brillouin scattering in singlemode optical fibers," *Phys. Rev. B*, vol. 19, pp. 4986–4998, May 1979.

[5] J. Nagel *et al.*, "Experimental investigation of silicate-glass-based Raman gain fibers with enhanced SBS suppression by selective transverse doping," *J. Lightw. Technol.*, vol. 34, no. 3, pp. 928–942, Feb. 2016.

[6] Y. Koyamada, S. Sato, S. Nakamura, H. Sotobayashi, and W. Chujo, "Simulating and designing brillouin gain spectrum in singlemode fibers," *J. Lightw. Technol.*, vol. 22, no. 2, pp. 631–639, Feb. 2004.

[7] B. Ward and J. Spring, "Finite element analysis of brillouin gain in SBS-suppressing optical fibers with non-uniform acoustic velocity profiles," *Opt. Express*, vol. 17, pp. 15685–15699, Aug. 2009.

[8] S. Yoo, C. A. Codemard, Y. Jeong, J. K. Sahu, and J. Nilsson, "Analysis and optimization of acoustic speed profiles with large transverse variations for mitigation of stimulated brillouin scattering in optical fibers," *Appl. Opt.*, vol. 49, pp. 1388–1399, Mar. 2010.

[9] M. D. Mermelstein, M. J. Andrejco, J. Fini, A. Yablon, C. Headley, and D. J. DiGiovanni, "11.2 dB SBS gain suppression in a large mode area Yb-doped optical fiber," *Proc. SPIE*, vol. 6873, 2008, pp. 68730N1–68730N7.

[10] T. Hosaka, Y. Sasaki, K. Okamoto, and J. Noda, "Stress-applied polarization-maintaining optical fibers. Design and fabrication," *Electron. Commun. Japan*, vol. 68, pp. 37–47, 1985.

[11] M. M. Khudyakov *et al.*, "Optimisation of an acoustically antiguiding structure for raising the stimulated brillouin scattering threshold in optical fibres," *Quantum Electron.*, vol. 46, pp. 468–472, 2016.

[12] L. Dong, "Limits of stimulated brillouin scattering suppression in optical fibers with transverse acoustic waveguide designs," *J. Lightw. Technol.*, vol. 28, no. 21, pp. 3156–3161, Nov. 2010.

[13] M. M. Khudyakov *et al.*, "Singlemode large-mode-area er–yb fibers with core based on phosphorosilicate glass highly doped with fluorine," *Laser Phys. Lett.*, vol. 16, pp. 025105–025111, Jan. 2019.

[14] R. W. Boyd, "Chapter 9. Stimulated brillouin and stimulated rayleigh scattering," in *Nonlinear Optics*. 3rd ed. New York, NY, USA: Elsevier, 2008, pp. 429–471.

[15] G. Agrawal, "Chapter 9. stimulated brillouin scattering," in *Nonlinear Fiber Optics*, 5th ed. Amsterdam: Elsevier, 2013, pp. 353–396.

[16] A. Kobyakov, S. Kumar, D. Q. Chowdhury, A. Boh Ruffin, M. Sauer, and S. R. Bickham, "Desing concept for optical fibers with enhanced SBS threshold," *Opt. Express*, vol. 13, pp. 5338–5346, Jun. 2005.

[17] C.-K. Jen, C. Neron, A. Shang, K. Abe, L. Bonnell, and J. Kushibiki, "Acoustic characterization of silica glasses," *J. Am. Ceram. Soc.*, vol. 76, pp. 712–716, 1993.

[18] N. Shibata, K. Okamoto, and Y. Azuma, "Longitudinal acoustic modes and Brillouin-gain spectra for geo2-doped-core singlemode fibers," *J. Opt. Soc. Am. B*, vol. 6, pp. 1167–1174, Jun. 1989.

[19] A. Bertholds and R. Dändliker, "Determination of the individual strain-optic coefficients in singlemode optical fibres," *J. Lightw. Technol.*, vol. 6, pp. 17–20, Jan. 1988.

[20] M. M. Bubnov *et al.*, "Fabrication and investigation of singlemode highly phosphorus-doped fibers for raman lasers," in *Proc. SPIE*, vol. 4083, Advances in Fiber Optics, May 2000, pp. 12–22.

[21] W. Hermanna and D.U. Wiechert, "Refractive index of doped and undoped PCVD bulk silica," *Mat. Res. Bull.*, vol. 24, pp. 1083–1097, Sep. 1989.

[22] P.-C. Law, Y.-S. Liu, A. Croteau, and P. D. Dragic, "Acoustic coefficients of P_2O_5-doped silica fiber: Acoustic velocity, acoustic attenuation, and thermo-acoustic coefficient," *Opt. Express*, vol. 1, pp. 686–699, Jul. 2011.

[23] M. Niklès, L. Thévenaz, and P. A. Robert, "Brillouin gain spectrum characterization in single mode optical fibers," *J. Lightw. Technol.*, vol. 15, no. 10, pp. 1842–1851, Oct. 1997.

[24] J. W. Fleming and D. L. Wood, "Refractive index dispersion and related properties in fluorine doped silica," *Appl. Opt.*, vol. 22, pp. 3102–3104, 1983.

[25] M. Dämmig, G. Zinner, F. Mitschke, and H. Welling, "Stimulated brillouin scattering in fibers with and without external feedback," *Phys. Rev. A*, vol. 48, pp. 3301–3309, Oct. 1993.

[26] L.V. Kotov *et al.*, "Record-peak-power all-fiber single-frequency 1550 nm laser," *Laser Phys. Lett.*, vol. 11, pp. 095102–095107, 2014.
[27] M. M. Khudyakov, M. E. Likhachev, M. M. Bubnov, D. S. Lipatov, A. S. Lobanov, and A. N. Guryanov, "Three layer fiber with high stimulated brillouin scattering threshold," *Proc. SPIE*, vol. 10083, San Francisco, USA, Feb. 2017, Art. no. 1008313.
[28] M. O. van Deventer and A. J. Boot, "Polarization properties of stimulated brillouin scattering in singlemode fibers," *J. Lightw. Technol.*, vol. 12, no. 4, pp. 585–590, Apr. 1994.

Sergey. V. Tsvetkov received the M.S. degree in precision engineering from the Moscow State Academy of Instrument Engineering and Informatics . From 2003 to 2015, he was employed there at the Department of Physics as a Senior Lecturer and the Head of the laboratory. In 2019, he joined the Dianov Fiber Optics Research Center. His scientific research interests include the fundamental theory and calculation of optical fibers, including the modeling of nonlinear processes in fiber optics.

Maxim M. Khudyakov received the B.S. and M.S. degrees in physical engineering from the Moscow Institute of Physics and Technology, in 2015 and 2017, respectively. He joined the Fiber Optics Research Center of Russian Academy of Sciences, Dianov Fiber Optics Research Center, in 2014. His research activities are connected with the fabrication and investigation of fibers with suppressed stimulated Brillouin scattering.

Alexey S. Lobanov received the M.S. degree in general physics from the N.P.Ogarev Mordovia State University, in 2004, and the Ph.D. degree in chemistry, in 2013. He is currently working with the Institute of Chemistry of High Purity Substances of the Russian Academy of Sciences as a Staff Researcher. His current research interests include development and manufacturing of specialty optical fibers with MCVD technology.

Denis S. Lipatov received the graduate degree from Mordovian State University, Saransk, Russia, in 2003, the major is chemistry. Then, he joined the Institute of Chemistry of High-Purity Substances of the Russian Academy of Sciences. In 2010, he received the Ph.D. degree in chemistry. His research activities are connected with the development of novel silica-based glass for specialty fibers, including active fibers, and large-mode-area fibers**.**

Mikhail M. Bubnov received the Graduate degree from the M.V. Lomonosov Moscow State University in 1970 to join the P.N. Lebedev Physical Institute (LPI) of the Academy of Sciences of the USSR. He received the Ph.D. and D.Sc. degrees in 1978 and 2009, respectively. He is a Corresponding Member of the Russian Academy of Sciences. He is currently working with the Fiber Optics Research Center as a Leading Research Fellow. His current research interests include the development of new types of optical fibers, the investigation of rare-earth ion clustering, and the photo darkening of Yb-doped fibers.

Alekxey N. Guryanov received the graduate degree from the Lobachevsky State University of Nizhni Novgorod, Nizhny Novgorod, Russia, in 1967. In 1974, he received the Ph.D. degree in chemistry. In 1988, he received the D.Sc. degree in chemistry. He is a Corresponding Member of the Russian Academy of Sciences. He is currently the Head of Laboratory with the Institute of Chemistry of High Purity Substances, Russian Academy of Sciences. His current research interests include development of specialty optical fibers using MCVD technology.

Valery Temyanko received the M.S. degree in chemical engineering from Louisiana State University, Baton Rouge, in 1997. In 2000, he joined the University of Arizona, Tucson, where he is a Staff Engineer. His research activities include manufacturing of micro- and nanostructured fibers, fiber lasers, electro–optic modulators, couplers, and switches.

Mikhail E. Likhachev received the B.S. and M.S. degrees in physical engineering from the Moscow Institute of Physics and Technology, in 1999 and 2001, respectively. In 2005, he received the Ph.D. degree and his position at FORC RAS is currently the Head of Laboratory. He joined the Dianov Fiber Optics Research Center in 1999. His research activities are connected with the fabrication and investigation of new types of special fibers: Bragg and hybrid fibers, fibers doped with rare-earth ions, novel types of large-mode-area fibers, highly Ge-doped and P-doped fibers, etc.